We are IntechOpen, the world's leading publisher of Open Access books Built by scientists, for scientists

6,900
Open access books available

185,000
International authors and editors

200M
Downloads

Our authors are among the

154
Countries delivered to

TOP 1%
most cited scientists

12.2%
Contributors from top 500 universities



WEB OF SCIENCE™

Selection of our books indexed in the Book Citation Index in Web of Science™ Core Collection (BKCI)

Interested in publishing with us?
Contact book.department@intechopen.com

Numbers displayed above are based on latest data collected.
For more information visit www.intechopen.com



Chapter

Diffractive Corneal Inlays: A New Concept for Correction of Presbyopia

Diego Montagud-Martínez, Vicente Ferrando, Salvador Garcia-Delpech, Juan A. Monsoriu and Walter D. Furlan

Abstract

A new class of corneal inlays for treatment of presbyopia is described, which uses diffraction as the working principle. The inlay consists of an opaque disk with a small central aperture surrounded by an array of micro-holes that are distributed following the order of a given Fresnel zone plate having N zones. In this way, the central hole of the disk produces an extension of the depth of focus of the eye for distance vision and contributes to the zero order of diffraction, and the light diffracted by the micro-holes in the periphery produces a real focus for near vision. In our general design, the number of zones and the diameter of the central hole are free parameters that can be used to design customized devices with different addition power and near-focus intensity. Two different designs are analyzed to show this property. In the analysis, we employed a ray tracing software to study the performance of the new inlays in the two different model eyes. The results are compared with those obtained with a model of the small-aperture inlay that is currently in the market. The different merit functions used in the comparison and the image simulations performed with the inlays in the model eyes show the excellent performance of our proposal.

Keywords: presbyopia, corneal inlay, diffractive optics, refractive surgery, cornea

1. Introduction

Affecting approximately 2 billion people worldwide, presbyopia is the most common refractive defect in the population, disturbing the quality of life of people over 45 years. It is expected that this situation will grow to reach 2100 million in 2020 [1]. In fact, presbyopia is a natural condition of the human being due to aging, and it is caused by the loss of ability of the crystalline lens to accommodate.

The treatment of presbyopia has historically been addressed from multiple perspectives: spectacles (reading glasses, bifocals, and progressive), multifocal contact lenses, and refractive surgery. Within this area, the most recent surgical approach is in the use of corneal inlays (CIs) [1, 2]. These implants consist of lenticels of a biocompatible synthetic material that, as the name implies, are placed into the corneal stroma. The main advantage of CI over other surgical therapies, like intraocular lenses, is that it is a minimally invasive and reversible surgery [3]; in addition, CIs are stable and do not require maintenance.

Currently, all CIs are implanted monocularly in the nondominant eye producing a modified variant of the monovision system, which consists in using the dominant eye for distance vision and the nondominant one for intermediate-near vision. Commercial examples of CIs are the Flexivue Microlens® (Presbia Cooperatief, UA, Irvine, CA, USA) [1, 4, 5], the Raindrop® (ReVision Optics, Lake Forest, CA, USA) [1, 5, 6], and the small-aperture corneal inlay (SACI) whose trade name is KAMRA® inlay (Acufocus, Inc., Irvine, CA, USA) [1, 5, 7–10]. The principle of operation of each model is different. The Flexivue inlay is a bifocal device of the center-far type, since it has a central hole for the passage of nutrients that allows the vision of far and a peripheral area for the near vision that contains the power of addition. The Raindrop inlay uses a different refractive principle, which consists of introducing a lenticel of permeable material in the center of the corneal stroma to create a hyperprolate cornea. Therefore, the cornea becomes itself a center-near bifocal lens. Finally, the SACI uses the pinhole effect to extend the depth of focus of the eye in far vision. Indeed, it consists of an opaque ring of 1.6 mm internal diameter and 3.6 mm external diameter, constructed with carbon-doped polyvinylidene fluoride. It has about 8400 micro-holes with diameters between 5 and 10 μm, distributed randomly to allow the passage of nutrients through the stroma, which gives it around 5% transmittance [10]. Surgically, it is introduced at a depth of 200 μm. The SACI is the most successful commercial CI and has been widely studied both clinically and theoretically [1, 5, 7–10]. However, it has certain drawbacks. As it is an opaque ring, the amount of light that reaches the retina of each eye is different, causing a degradation of binocular distance visual acuity [11] and a potential detrimental effect on the binocular summation ratio [12]. Moreover, the SACI produces marked interocular differences in visual latency and a Pulfrich effect [13]. Other visual function that is compromised by the SACI is a deterioration in stereoacuity with respect to natural conditions, especially for near and intermediate distances [14].

In this chapter we describe a new concept of CI developed by our research group that is based on the concept of diffraction. It consists of a variation of an amplitude Fresnel zone plate [15] in which micro-holes conform the clear zones of the zone plate in a similar way as was proposed to construct the so-called photon sieves [16]. Photon sieves were conceived for its use in X-ray microscopy but were also found to have numerous applications in various scientific and technological areas [17–19]. Inspired by this concept, we conceived the first diffractive corneal inlay (DCI) in which the distribution of holes in an opaque ring has been ordered to achieve a bifocal intrastromal lens. In this way, the light diffracted by the inlay (an unwanted effect in the SACI commercial design) generates a focus, which would allow presbyopic patients to see close objects clearly. To demonstrate its properties, in the following sections theoretical and numerical results are compared with the SACI, using two different theoretical eye models implemented in the ZEMAX™ OpticStudio software (EE version 18.7, ZEMAX Development Corporation, Bellevue, Washington, USA). To evaluate the optical quality of ICs, the modulation transfer function (MTF), which defines the visibility of a given optical system for all spatial frequencies [20]; the area under the MTF curve (AMTF), computed for different object vergences; and the point spread function (PSF) [20] that describes the response of an optical system to a point source have been used. In addition, the numerically calculated PSFs have been used to obtain simulated images of an optotype test chart.

2. Diffractive corneal inlay (DCI)

The starting point of the DCI design is an amplitude Fresnel zone plate, which has been devised with the optical power necessary to generate the addition. In it, instead of fully transparent zones, micro-holes are made to allow the passage of

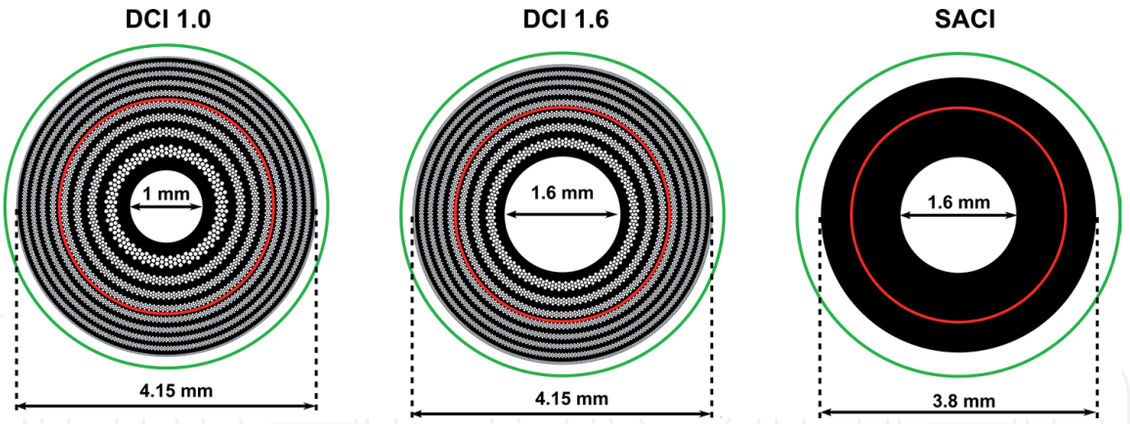


Figure 1.
Design of the analyzed DCIs and the SACI.

light and the nutrients, forming a single structure without any substrate. The DCI [21], in addition to presenting the aforementioned micro-hole structure, has a central hole that acts as a pinhole of variable diameter; thus the DCI presents different diffractive orders. The zero order focuses the light for distant vision, while the +1 order forms the near focus. By varying the number of rings, the number and size of the micro-holes, as well as the internal diameter of the central hole, the diffraction efficiency of the far, and near foci can be modified.

Here we evaluated two DCI models in comparison with a SACI with the dimensions of the KAMRA® (see **Figure 1**). Both DCIs were designed to provide a near focus corresponding to an addition of +2.50 D, and both have an external diameter of 4.15 mm. DCI 1.0 has a central hole of 1.00 mm diameter surrounded by 8 rings with a total of 6394 holes. DCI 1.6 was designed with a central hole of 1.6 mm diameter surrounded by 7 rings conformed by a total of 5989 holes. A complete opaque with the dimensions of the SACI, as shown in **Figure 1**, was evaluated in parallel for comparison.

3. Focusing properties: axial irradiance

To evaluate the focusing properties of the DCIs, we first computed the axial irradiances provided by them in air under monochromatic illumination for a wavelength of 555 nm using the Fresnel approximation [9]. **Figure 2** shows the

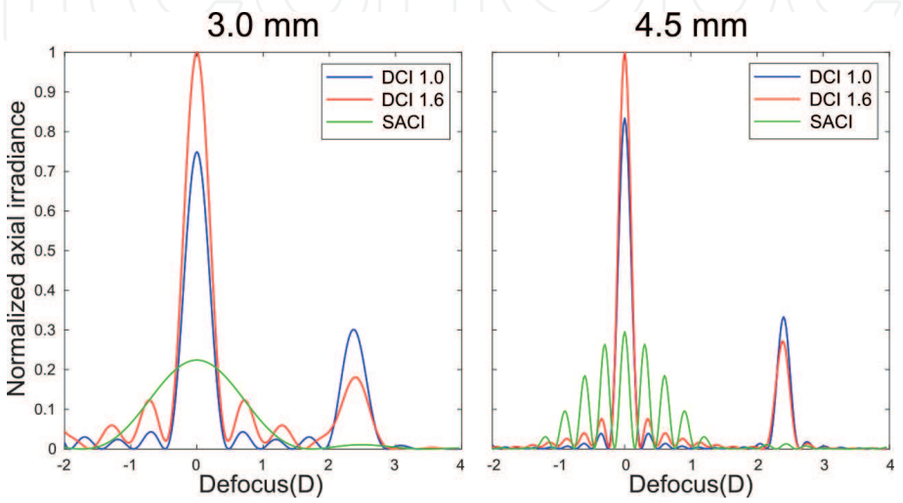


Figure 2.
Normalized axial irradiances of the three CIs for pupil diameters of 3.0 mm (left) and 4.5 mm (right).

results, computed for CIs with external pupils of 3.0 and 4.5 mm diameter (see the red and green circles in **Figure 1**). As can be seen, the profile of the DCIs is clearly bifocal, while that of the SACI is, as expected, of a typical extended focus one. Note also that both DCIs have a more intense focus than the SACI in distant vision (zero defocus).

4. MTFs and AMTFs

The MTFs and AMTFs of the inlays have been calculated using the ZEMAX™ OpticStudio software, in which two theoretical eye models have been implemented: the Liou-Brennan Model Eye (LBME) [22] and the ZEMAX Model Eye (ZME) [23].

The ZME is an eye model included in the software package. **Table 1** shows the data sheet used for the simulations with the ZME.

The LBME is one of the most popular theoretical models because it has the most realistic biometrical data obtained from 45-year-old people (young presbyopes). It takes into account the alpha angle [22] (the angle between the visual axis and the optical axis), the 0.5-mm nasal displacement of the pupil, and the gradient refractive index of the crystalline lens. Its optical parameters are shown in **Table 2**. The major difference between both models relies in the corneal asphericities (Q) that induce different values for the spherical aberration (SA) in each eye.

Surface	Radius (mm)	Asphericity (Q)	Thickness (mm)	Refractive index
Anterior cornea	7.80	−0.50	0.200	1.377
Anterior CI	7.80	−0.50	0.005	1.377
Posterior CI	7.80	−0.50	0.315	1.377
Posterior cornea	6.70	−0.30	3.100	1.337
Iris	—	—	0.100	1.337
Anterior lens	10.00	0.00	3700	1420
Posterior lens	−6.00	−3.25	16.580	1.336

Table 1.
Parameters of ZME.

Surface	Radius (mm)	Asphericity (Q)	Thickness (mm)	Refractive index
Anterior cornea	7.77	−0.18	0.200	1.376
Anterior CI	7.77	−0.18	0.005	1.376
Posterior CI	7.77	−0.18	0.295	1.376
Posterior cornea	6.40	−0.60	3.16	1.336
Iris	—	—	0.00	—
Anterior lens	12.4	−0.94	1.59	$1.368 + 0.049057\,z - 0.015427\,z^2 - 0.001978\,r^2$
Lens	Infinity	—	2.43	$1.407 - 0.006605\,z^2 - 0.001978\,r^2$
Posterior lens	−8.10	0.96	16.26	1.336

Table 2.
Parameters of LBME, the pupil is decentered 0.5 mm nasally, and the incidental beams have an angle of entry of 5°.

In these model eyes, both DCIs and the SACI have been inserted virtually at a distance of 200 μm from the anterior surface of the cornea, simulating the surgical procedure of the SACI [5]. In the simulation in ZEMAX, the inlays have been introduced as *.uda* (user-defined aperture) files. To simulate a thickness of 5 μm for the CIs, two CI surfaces were introduced into each eye model, as can be seen in **Tables 1** and **2**. The CIs were centered on the visual axis of each model eye.

The MTFs have been calculated for far and near foci and also for different vergences between +0.50 D and − 3.50 D in steps of 0.10 D, in order to calculate the AMTF. The AMTFs have been obtained integrating the MTF values for a frequency range from 9.49 to 59.86 cycles per degree (cpd), corresponding to visual acuities (VA) between 0.5 logMAR and −0.2 logMAR, respectively.

Figure 3 shows the MTFs at the far and near foci for 3.0-mm pupils. As can be seen, both model eyes predict a similar behavior for the three ICs in both far and near foci. It should be mentioned that for the LBME, the represented MTFs in **Figure 3** are computed as the mean values between the sagittal and the tangential MTF curves. In addition, as explained in previous sections, the higher internal diameter of the DCI 1.6 causes a higher amount of light that focuses on the far distance image with respect

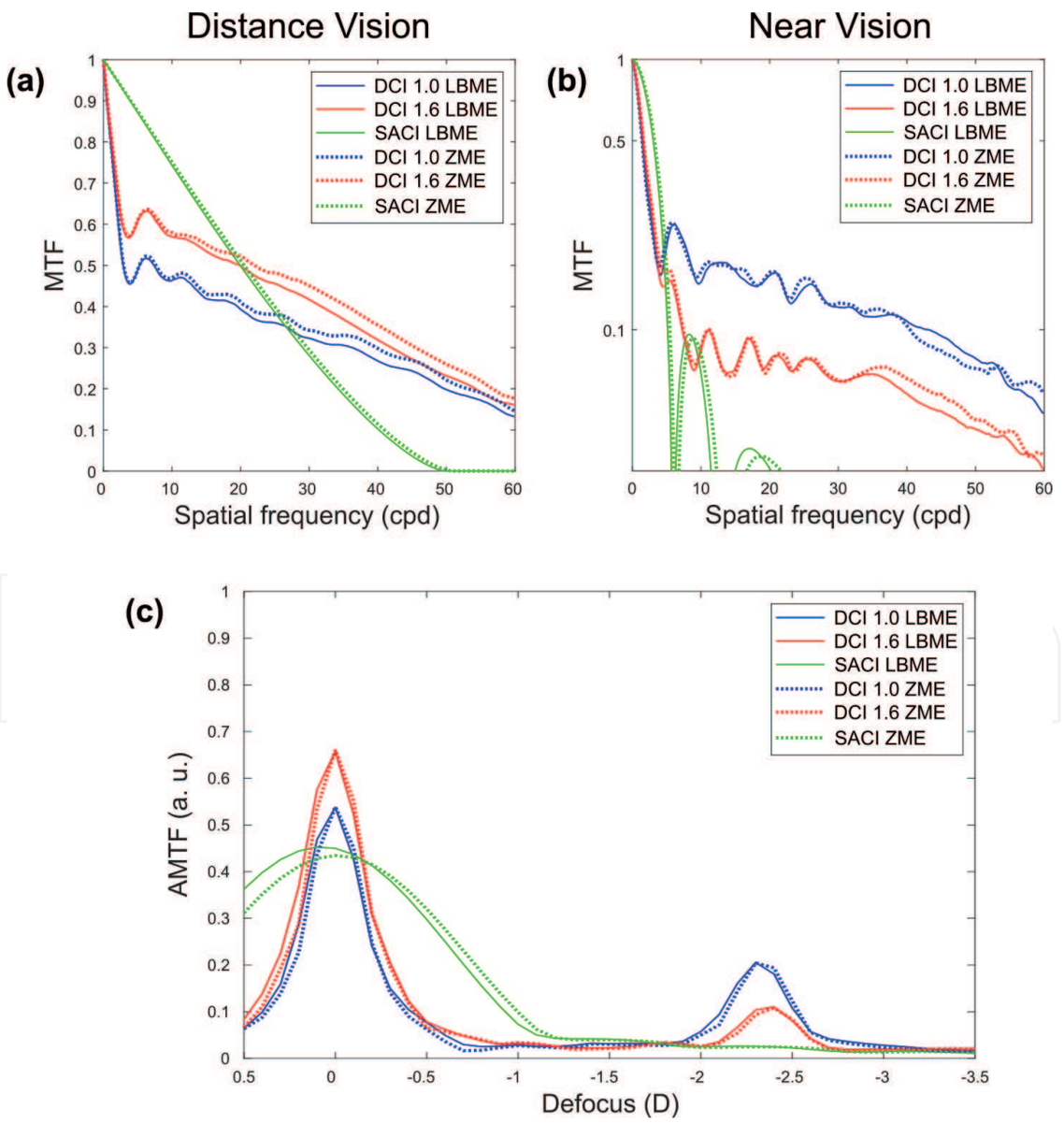


Figure 3.
A 3.0-mm pupil: (a) MTF distance vision, (b) MTF near vision, and (c) AMTF for different defocus conditions of the three CIs: DCI 1.0 (blue), DCI 1.6 (red), and SACI (green) for LBME (continuous lines) and ZME (dashed lines).

to the DCI 1.0. For this reason, the MTF at the far focus of the DCI 1.6 is the better one. The opposite is true for the near focus, while SACI theoretically presents an extended focus, as can be seen in the AMTF; it does not have a defined focus for near vision. In contrast, the diffractive profile of the DCIs generates the near focus that can be seen in **Figure 3c**. The MTF for the near-vision focus of DCI 1.0 is better than for DCI 1.6 because the total area of the inlay is higher. On the other hand, differences between both eye models are hardly observed, because for a 3.0-mm pupil, the influence of the LBME asymmetry and the SA is both minimal.

Figure 4 shows the same merit functions as in **Figure 3** but is calculated for 4.5-mm pupils. The influence of the SA on the eye models can be seen in **Figure 4c**. While the AMTFs of the three CIs in the ZME maintain their focus of vision at distance (zero defocus), in the LBME, the AMTF peaks of the far focus are shifted 0.1 D due to the influence of the SA; however, in the near focus, this effect is not so obvious. It is important to note the effect of the pupil size on the depth of focus of the inlays. As can be seen in the comparison between **Figure 3c** and **4c**, the AMTF

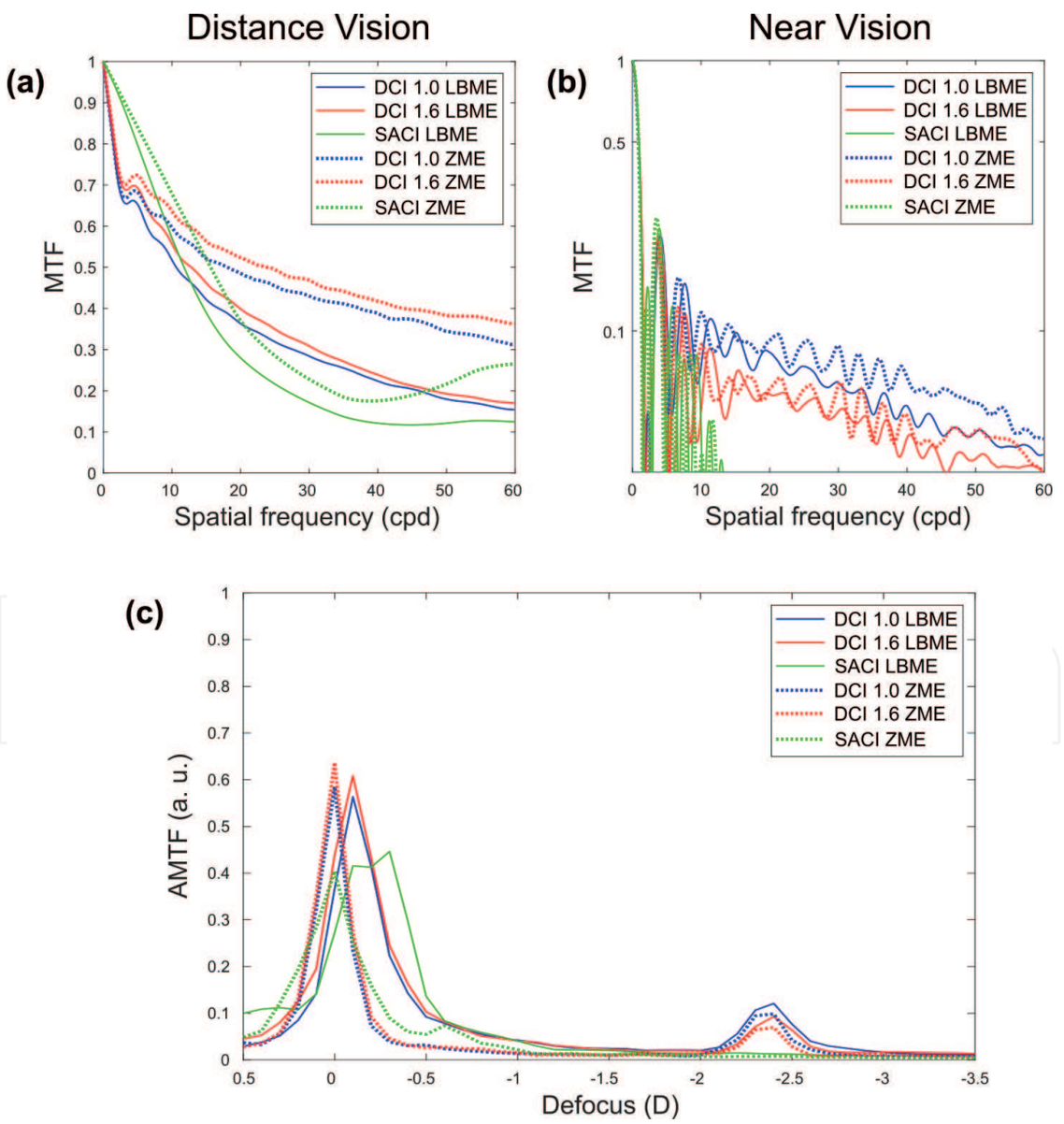


Figure 4.
A 4.5-mm pupil: (a) MTF distance vision, (b) MTF near vision, and (c) AMTF for different defocus conditions of the three CIs: DCI 1.0 (blue), DCI 1.6 (red), and SACI (green) for LBME (continuous lines) and ZME (dashed lines).

of both ICDs is less affected than the AMTF of the SACI, since for the latter the depth of focus is severely reduced.

5. PSF and image simulation

As stated above, the PSF describes the ability of an optical system (in our case an eye model with a CI) to form a good image of a point source. An ideal PSF corresponds to a diffraction-limited system and is known as the airy disk, with a high-intensity central peak, which is more or less concentrated depending on the pupil size. For real systems the PSF spreads out; as more extended is the PSF, the system is worse.

Figures 5 and **6** show the PSFs obtained for the 3.0 and 4.5-mm pupils, respectively, of the three ICs in both eye models. PSFs calculated with ZEMAX were weighted according to the axial irradiances calculated in Section 3 for each CI. Considering that the foci in distance and in near vision have different range intensities, different normalizations were performed in order to compare them. In this way, the PSFs at the far and near foci are normalized to the maximum value of the DCI 1.6 PSF in the ZME, and the PSFs of the near-vision focus are normalized to the maximum of the PSF of the near-focus DCI 1.6 of the ZME in each focus, respectively. This means that in **Figures 5** and **6**, the eye models of the three CIs in each focus can be only compared, but far and near PSFs have different normalizations.

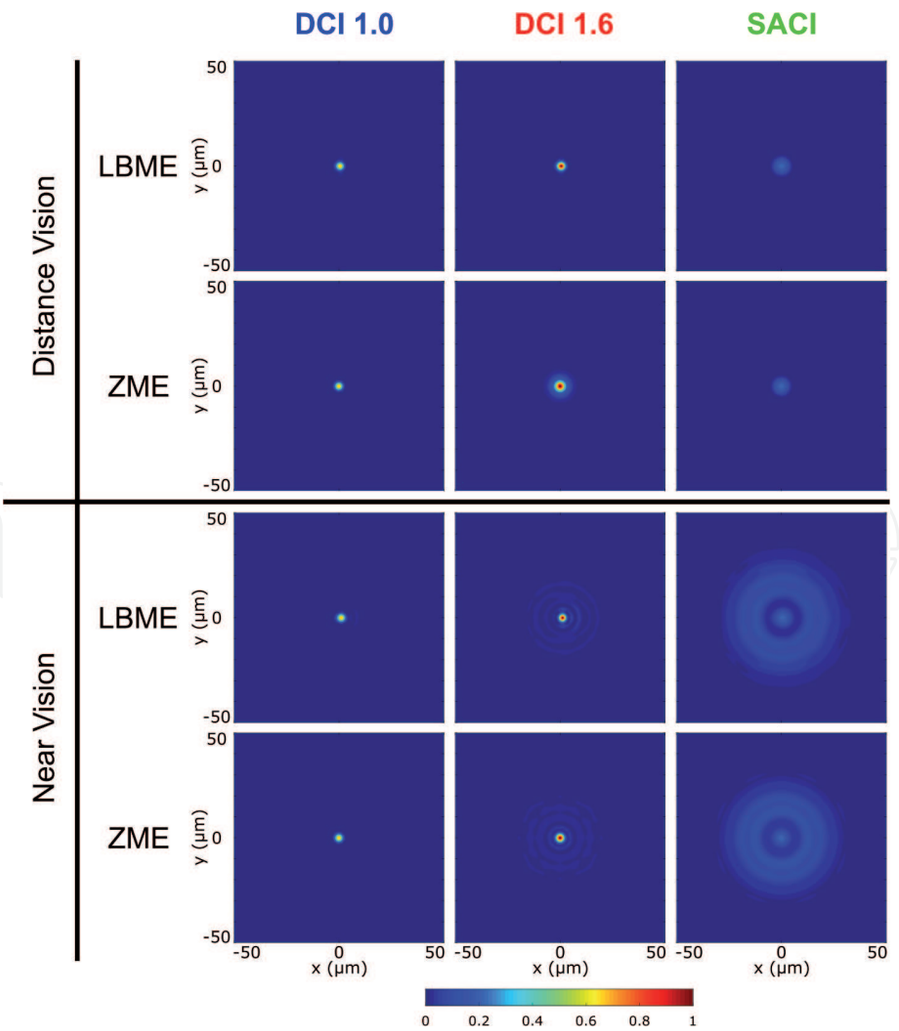


Figure 5.
PSFs normalized to the maximum of each triplet of CIs for pupil of 3.0 mm in distance vision (top) and near vision (bottom).

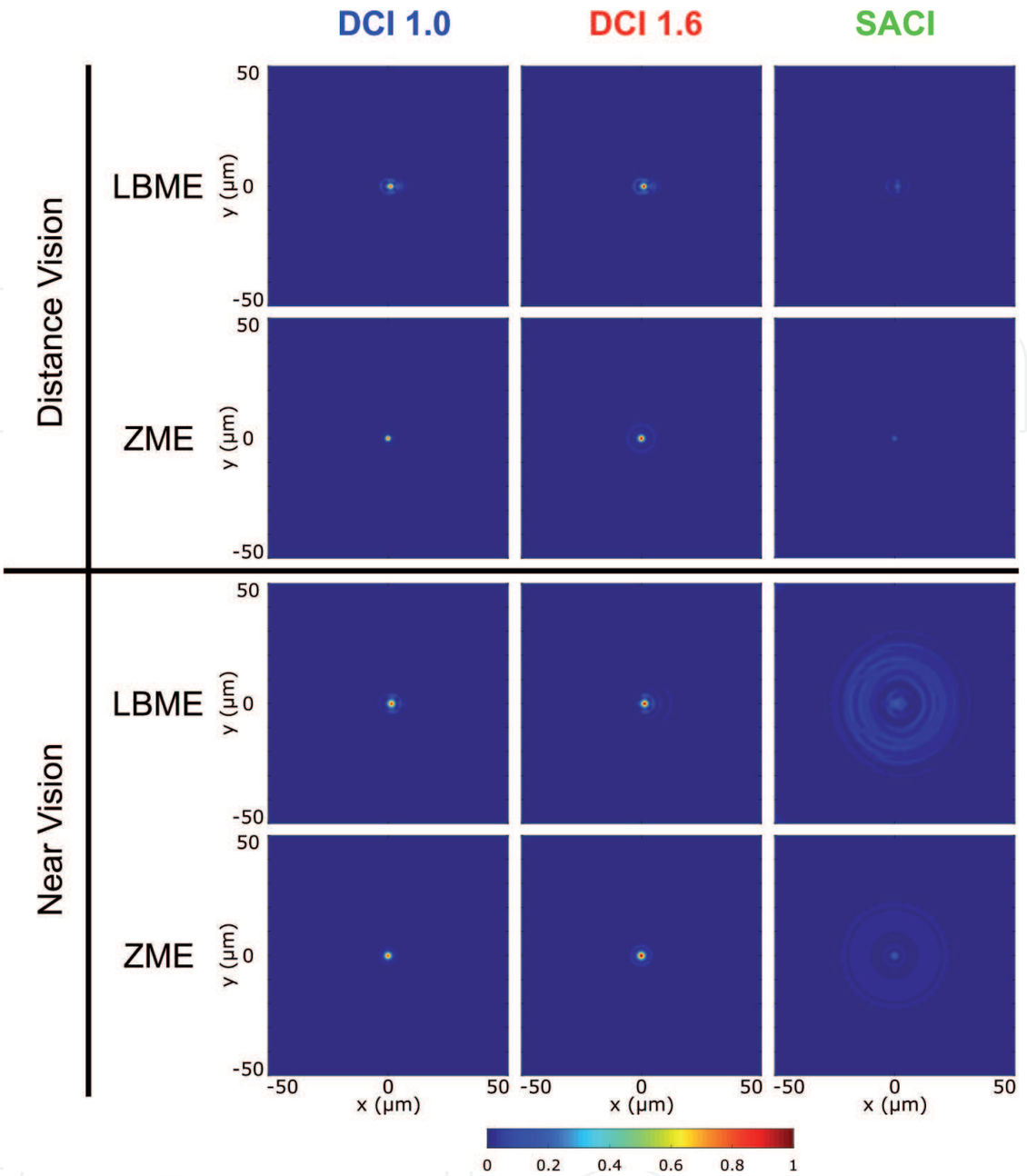


Figure 6.
PSFs normalized to the maximum of each triplet of CIs for pupil of 4.5 mm in distance vision (top) and near vision (bottom).

Figure 5 shows that, for both the LBME and the ZME in distance vision, DCI 1.6 has a more intense focus than the other two CIs, but it has a slightly wider peak than DCI 1.0. In near vision the same trend is shown, the maximum of the DCI 1.6 is higher than that of the other two CIs, but its surrounding halo is also more extended. Note that the SACI has an even greater halo. For 3.0-mm pupil at near vision, the first impression is that the PSF for DCI 1.6 is better than the one for DCI 1.0 PSF # 1; however, it should be borne in mind that, while the maximum value of the first one is the unity, the energy is very dispersed (the halo). In DCI 1.0, although the maximum is less than 0.802, the energy is more concentrated, and therefore the PSF is better. The explanation of why the PSF of DCI 1.6 is globally better is simple: the diffraction efficiency of DCI 1.6 is better, focusing more light on the near-vision focus. On the other hand, as expected, for 3.0-mm pupil diameter, the CIs' performance is similar in both eye models.

Figure 6 shows the same composition as **Figure 5** but with the 4.5-mm pupil. As we explained before, by increasing the pupil diameter, the influence of SA is higher on each eye model. On the one hand, a focal shift is produced, as already shown in **Figure 3c**, and on the other hand, the shape and height of the PSF are also affected. The comparison of the performance of both eye models for 4.5-mm pupil diameter shows more noticeable differences than those observed with the small pupil. In all cases, the LBME has more extended and asymmetrical halos than ZME. This is due to the influence of the SA and also, to the asymmetry of the LBME.

Finally, after the quantitative comparison of the merit functions for the three CIs, images of an optotype chart have been simulated. To this end, the PSFs obtained from ZEMAX were normalized to their respective maximum values and then weighed by the axial irradiances of each IC calculated in Section 3. These normalized and weighted PSFs were convolved with Landolt C optotypes corresponding to three different values of VA: 0.4 logMAR, 0.2 logMAR, and 0.0 logMAR.

Figures 7 and **8** show simulated images for 3.0 and 4.5-mm pupil diameters, respectively. For 3.0-mm pupil, it can be seen that, while the DCIs have a greater contrast than the SACI, the resolution of the three ICs is similar because the extension of the corresponding PSFs are almost the same (see **Figure 5**). At the near focus, it is observed that there is no focus on SACI, but in DCI 1.0 although the contrast is lower, the resolution is higher, and the halo is smaller than for DCI 1.6. When comparing the performance of the eye models, as already mentioned, there are no significant differences because when using a small pupil, the influence of high-order aberrations is minimal.

The simulated images for 4.5-mm pupil are shown in **Figure 8**. It can be seen that the differences between the eye models are most noticeable, mainly in the halos in near vision. The halos of the ZME are symmetrical, while those of the LBME are not. Despite these differences, the behavior of the three CIs maintains the same trend. The images at the foci for both DCIs are comparable in contrast

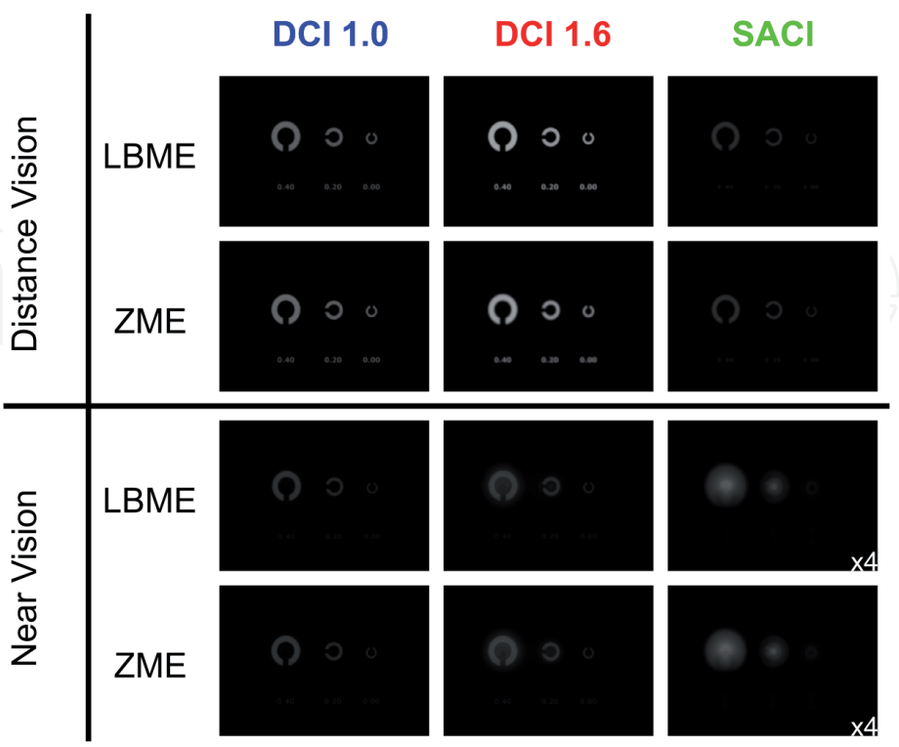


Figure 7.
Image simulation for 3.0 mm of pupil in distance vision (top) and near vision (bottom) for the three Cis in the two model eyes. The intensity of the image simulation of SACI in near vision has been multiplied 4×.

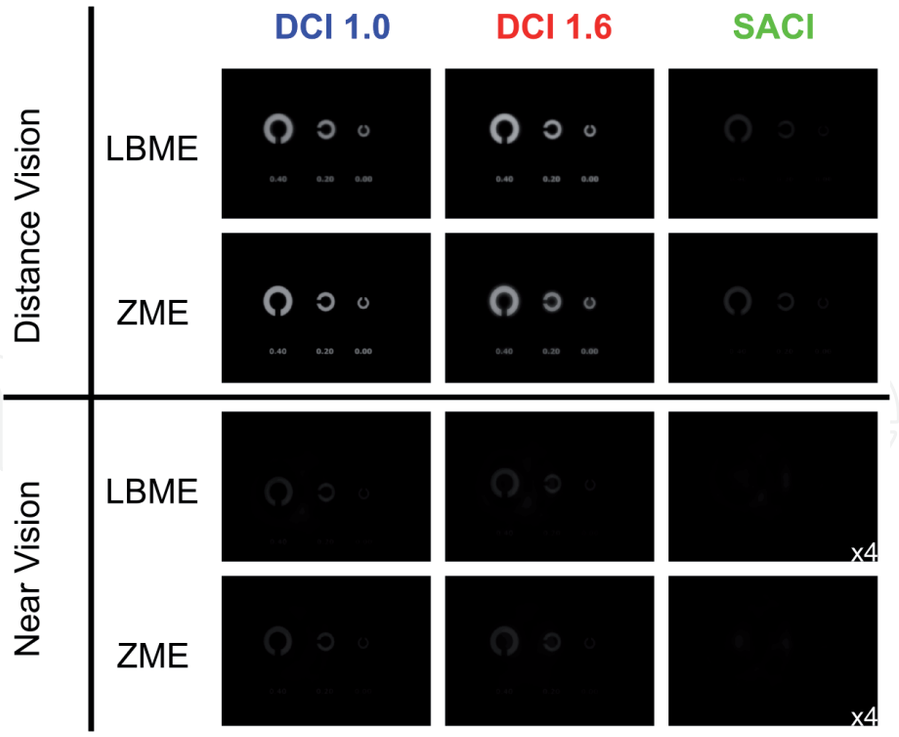


Figure 8.
Image simulation for 4.5 mm of pupil in distance vision (top) and near vision (bottom) for the three CIs in the two model eyes. The intensity of the image simulation of SACI in near vision has been multiplied 4×.

and definition. The reason that they resemble for distance vision is because with a large pupil, a part of the light that passes outside the inlays (external diameter of 4.15 mm) goes to the far focus. Therefore, the intensity ratio between the far and near foci increases and is similar for both DCIs.

By comparing both pupils, the best foci in the distance are for the DCIs with 4.5-mm pupil. The best focus for near vision is the DCI 1.0 since it presents more diffractive rings contributing to the near focus.

6. Conclusions

We have demonstrated that both DCI designs have a clearly bifocal profile due to their diffractive nature. Moreover, they also have better MTFs and AMTFs than the SACI (see **Figures 3** and **4**). The results presented in this chapter confirm the versatility of the DCI design because, opposite at what happens for the SACI which only presents a fixed depth focus, the distribution of the holes in the DCI can be modified (customized) to alter the relationship between the far- and near-vision foci. It is also verified that while for the 3.0-mm pupil, the three CIs have a similar behavior in both eye models, for 4.5 mm the differences are more due to the high-order aberrations of each model.

The PSFs show the differences between each CI for each situation; on the one hand, the DCIs generally show higher peaks and a high energy concentration and less extension of the PSF, but higher than SACI. These results can be clearly appreciated in the simulated images shown in **Figures 7** and **8**.

In summary, the DCI is a diffractive CI that combines the principle of operation of the small-aperture inlay, for the central hole, with the diffraction generated by the micro-holes in the ring to generate a focus in near vision. The micro-holes allow the construction of a single-piece inlay able to be inserted into the corneal stroma allowing nutrients to pass through it. The results show that the light throughput of

the DCI is higher than the SACI, in addition to better PSFs and simulated images. In addition, we have demonstrated the differences that can be obtained in the results (light distribution between the foci) depending on the design of a DCI allowing to customize the CI for each patient based on their visual needs.

However, since it is a numerical simulation work with a ray tracing program, studies in an optical bench and clinical trials with contact lenses, which include the structure of the DCIs, should be carried out in the future.

Acknowledgements

Funding: Ministerio de Economía y Competitividad (DPI2015-71256-R); Generalitat Valenciana (PROMETEO/2019/048).

D. Montagud-Martínez and V. Ferrando acknowledge the financial support from the Universitat Politècnica de València, Spain (fellowships FPI-2016 and PAID-10-18, respectively).

D. Montagud-Martínez acknowledges the financial support from the Universitat Politècnica de València, Spain (fellowship FPI-2016).

Conflict of interest

The authors declare no conflict of interest.

Author details

Diego Montagud-Martínez[1*], Vicente Ferrando[1], Salvador Garcia-Delpech[2], Juan A. Monsoriu[1] and Walter D. Furlan[3]

1 Universitat Politècnica de València, Valencia, Spain

2 Hospital Universitari i Politècn ic La Fe, Valencia, Spain

3 Universitat de València, Valencia, Spain

*Address all correspondence to: diemonma@upvnet.upv.es

IntechOpen

© 2019 The Author(s). Licensee IntechOpen. This chapter is distributed under the terms of the Creative Commons Attribution License (http://creativecommons.org/licenses/by/3.0), which permits unrestricted use, distribution, and reproduction in any medium, provided the original work is properly cited. CC BY

References

[1] Arlt EM, Krall EM, Moussa S, Grabner G, Dexl AK. Implantable inlay devices for presbyopia: The evidence to date. Clinical Ophthalmology. 2015;**9**:129-137

[2] Charman WN. Developments in the correction of presbyopia II: Surgical approaches. Ophthalmic & Physiological Optics. 2014;**34**:397-426

[3] Lindstrom RL, Macrae SM, Pepose JS, Hoopes PC. Corneal inlays for presbyopia correction. Current Opinion in Ophthalmology. 2013;**24**(4):281-287 Flexivue solo

[4] Limnopoulou AN, Bouzoukis DI, Kymionis GD, et al. Visual outcomes and safety of a refractive corneal inlay for presbyopia using femtosecond laser. Journal of Refractive Surgery (Thorofare, N.J.: 1995). 2013;**29**(1):12-18. DOI: 10.3928/1081597X-20121210-01

[5] Moarefi MA, Bafna S, Wiley W. A review of presbyopia treatment with corneal inlays. Opthamology and Therapy. 2017;**6**(1):55-65

[6] Garza EB, Gomez S, Chayet A, Dishler J. One-year safety and efficacy results of a hydrogel inlay to improve near vision in patients with emmetropic presbyopia. Journal of Refractive Surgery (Thorofare, N.J.: 1995). 2013;**29**(3):166-172. DOI: 10.3928/1081597X-20130129-01

[7] KAMRA Inlay Restores Reading Vision [Internet]. [cited 14 August 2019]. Available from: https://kamra.com/

[8] Yilmaz ÖF, Bayraktar S, Agca A, Yilmaz B, McDonald MB, van de Pol C. Intracorneal inlay for the surgical correction of presbyopia. Journal of Cataract & Refractive Surgery. 2008;**34**(11):1921-1927

[9] Wating GOVI. Correction of presbyopia with a small aperture corneal inlay. Journal of Refractive Surgery. 2011;**27**(11):842-845

[10] Vilupuru S, Lin L, Pepose JS. Comparison of contrast sensitivity and through focus in small-aperture inlay, accommodating intraocular lens, or multifocal intraocular lens subjects. American Journal of Ophthalmology. 2015;**160**(1):150-162

[11] Vukich JA, Durrie DS, Pepose JS, Thompson V, van de Pol C, Lin L. Evaluation of the small-aperture intracorneal inlay: Three-year results from the cohort of the US Food and Drug Administration clinical trial. Journal of Cataract & Refractive Surgery. 2018;**44**(5):541-556

[12] Gilchrist J, Pardhan S. Binocular contrast detection with unequal monocular illuminance. Ophthalmic and Physiological Optics. 1987;7(4):373-377

[13] Plainis S, Petratou D, Giannakopoulou T, Radhakrishnan H, Pallikaris IG, Charman WN. Small-aperture Monovision and the Pulfrich experience: Absence of neural adaptation effects. PLoS One. 2013;**8**(10):e75987. DOI: 10.1371/journal.pone.0075987

[14] Castro JJ, Ortiz C, Jiménez JR, Ortiz-Peregrina S, Casares-López M. Stereopsis simulating small-aperture corneal inlay and Monovision conditions. Journal of Refractive Surgery. 2018;**34**(7):482-488

[15] Machado FJ, Monsoriu JA, Furlan WD. Fractal light vortices. In: Chapter from the Book Vortex Dynamics and Optical Vortices. 1st ed. Intech; 2017. 257 p. DOI: 10.5772/66343

[16] Kipp L, Skibowski M, Johnson RL, Berndt R, Adelung R, Harm S, et al.

Sharper images by focusing soft X-rays with photon sieves. Nature. 2001;**414**:184-188

[17] Menon R, Gil D, Barbastathis G, Smith HI. Photon-sieve lithography. Journal of the Optical Society A. 2005;**22**(2):342-345

[18] Andersen G. Large optical photon sieve. Optics Letters. 2005;**30**(22):2976-2978

[19] Giménez F, Monsoriu JA, Furlan WD, Pons A. Fractal photon sieve. Optics Express. 2006;**14**(25):11958-11963

[20] Artal P. Handbook of Visual Optics, Volume One: Fundamentals and Eye Optics. 2nd ed. CRC Press; 2017. 437 p. ISBN 9781482237856DISEÑO

[21] Furlan WD, García-Delpech S, Udaondo P, Remón L, Ferrando V, Monsoriu JA. Diffractive corneal inlay for presbyopia. Journal of Biophotonics. 2017;**10**(9):1110-1114. DOI: 10.1002/jbio.201600320

[22] Liou HL, Brennan NA. Anatomically accurate, finite model eye for optical modeling. Journal of the Optical Society A. 1997;**14**(8):1684-1695

[23] Zemax OpticStudio Knowledgebase—Zemax [Internet]. [cited 14 August 2019]. Available from: https://customers.zemax.com/os/resources/learn/knowledgebase/zemax-models-of-the-human-eye